Prompt and delayed γ spectroscopy of neutron-rich ^{94}Kr and observation of a new isomer

R.-B. Gerst,[1,*] A. Blazhev,[1] N. Warr,[1] J. N. Wilson,[2] M. Lebois,[2] N. Jovančević,[2] D. Thisse,[2] R. Canavan,[3] M. Rudigier,[3,4] D. Étasse,[5] E. Adamska,[6] P. Adsley,[2] A. Algora,[7] M. Babo,[2] K. Belvedere,[3] J. Benito,[8] G. Benzoni,[9] A. Boso,[10] S. Bottoni,[11,9] M. Bunce,[10] R. Chakma,[2] N. Cieplicka-Oryńczak,[12] S. Courtin,[13,14] M. L. Cortés,[15] P. Davies,[16] C. Delafosse,[2] M. Fallot,[17] B. Fornal,[12] L. M. Fraile,[8] D. Gjestvang,[18] A. Gottardo,[19] V. Guadilla,[17] G. Häfner,[1,2] K. Hauschild,[2] M. Heine,[13] C. Henrich,[4] I. Homm,[4] F. Ibrahim,[2] Ł. W. Iskra,[9,12] P. Ivanov,[10] S. Jazrawi,[3,10] A. Korgul,[6] P. Koseoglou,[4,20] T. Kröll,[4] T. Kurtukian-Nieto,[21] L. Le Meur,[17] S. Leoni,[11,9] J. Ljungvall,[2] A. Lopez-Martens,[2] R. Lozeva,[2] I. Matea,[2] K. Miernik,[6] J. Nemer,[2] S. Oberstedt,[22] W. Paulsen,[18] M. Piersa,[6] Y. Popovitch,[2] C. Porzio,[11,9,23] L. Qi,[2] D. Ralet,[24] P. H. Regan,[3,10] D. Reygadas-Tello,[25] K. Rezynkina,[26] V. Sánchez-Tembleque,[8] C. Schmitt,[13] P.-A. Söderström,[4] C. Sürder,[4] G. Tocabens,[2] V. Vedia,[8] D. Verney,[2] B. Wasilewska,[12] J. Wiederhold,[4] M. Yavachova,[27] F. Zeiser,[18] and S. Ziliani[11,9]

[1]*Institut für Kernphysik, Universität zu Köln, 50937 Köln, Germany*
[2]*Université Paris-Saclay, CNRS/IN2P3, IJCLab, 91405 Orsay, France*
[3]*Department of Physics, University of Surrey, Guildford GU2 7XH, United Kingdom*
[4]*Technische Universität Darmstadt, Fachbereich Physik, Institut für Kernphysik, 64289 Darmstadt, Germany*
[5]*LPC Caen, 6 Boulevard Maréchal Juin, 14000 Caen, France*
[6]*Faculty of Physics, University of Warsaw, PL 02-093 Warsaw, Poland*
[7]*IFIC, CSIC-University of Valencia, Valencia, Spain*
[8]*Grupo de Fisica Nuclear & IPARCOS, Universidad Complutense de Madrid, CEI Moncloa, 28040 Madrid, Spain*
[9]*INFN Sezione Milano, Via Celoria 16, 20133 Milano, Italy*
[10]*National Physical Laboratory, Hampton Road, Teddington, Middlesex TW11 0LW, United Kingdom*
[11]*Dipartimento di Fisica, Universitá degli Studi di Milano, Via Celoria 16, 20133 Milano, Italy*
[12]*Institute of Nuclear Physics, Polish Academy of Sciences, PL-31342 Krakow, Poland*
[13]*IPHC, 23 rue du Loess, 67037 Strasbourg, France*
[14]*CNRS, UMR7178, 67037 Strasbourg, France*
[15]*RIKEN Nishina Center, 2-1 Hirosawa, Wako, Saitama 351-0198, Japan*
[16]*School of Physics and Astronomy, University of Manchester, Oxford Road, Manchester M13 9PL, United Kingdom*
[17]*Subatech, IMT-Atlantique, Université de Nantes, CNRS-IN2P3, F-44307 Nantes, France*
[18]*University of Oslo, Department of Physics, P.O. Box 1048, Blindern, 0316 Oslo, Norway*
[19]*INFN Laboratori Nazionali di Legnaro, Viale dell'Universitá, 2, I-35020 Legnaro, Italy*
[20]*GSI Helmoltzzentrum für Schwerionenforschung GmbH, Planckstrasse 1, 64291 Darmstadt, Germany*
[21]*CENBG, UMR5797, Université de Bordeaux, CNRS, F-33170 Gradignan, France*
[22]*European Commission, Joint Research Centre, Directorate G for Nuclear Safety and Security, Unit G.2, 2440 Geel, Belgium*
[23]*TRIUMF, 4004 Wesbrook Mall, Vancouver, British Columbia, Canada V6T 2A3*
[24]*Grand Accélérateur National d'Ions Lourds, Bd Henri Becquerel, 14076 Caen, France*
[25]*School of Computing, Engineering and Mathematics, University of Brighton, Brighton BN2 4GJ, United Kingdom*
[26]*Institute for Nuclear and Radiation Physics, KU Leuven, 3000 Leuven, Belgium*
[27]*Institute for Nuclear Research and Nuclear Energy, Bulgarian Academy of Sciences, 1784 Sofia, Bulgaria*

(Received 16 April 2020; revised 22 October 2020; accepted 12 November 2020; published 24 December 2020)

Prompt and delayed γ-ray spectroscopy of the neutron-rich ^{94}Kr was performed, as part of the fission campaign at the ALTO facility of the IPN Orsay, using the fast-neutron-induced fission reaction ^{238}U(n, f) in combination with the ν-Ball array, a novel hybrid γ spectrometer for energy and lifetime measurements. Several new yrast and nonyrast transitions were observed for the first time, extending the previously known level scheme. Additionally, we report on the observation of a new short-lived isomer at 3444 keV with a half-life of 32(3) ns. The analysis of the Nilsson orbitals obtained from Gogny cranked Hartree-Fock-Bogoliubov calculations suggests a (9^-) spin and an oblate deformation for this isomer corresponding to a two-quasineutron state, indicating an isomeric structure very similar to that of the neighboring isotones ^{96}Sr and ^{92}Se.

DOI: 10.1103/PhysRevC.102.064323

*Corresponding author: rgerst@ikp.uni-koeln.de

I. INTRODUCTION

The study of nuclear properties far away from the valley of stability to investigate their dependence on the number of neutrons and protons is crucial to our understanding of the atomic nucleus and the nuclear forces. One important feature is the evolution of nuclear shape along the isotopic chains, which is determined by the interplay between the macroscopic and microscopic properties. In some mass regions, this interaction between collective and single-particle degrees of freedom can lead to a very sudden growth of collectivity. One way of interpreting this drastic behavior is within the context of the coexistence of two distinct configurations at low excitation energies, one spherical and one deformed, where the latter suddenly becomes energetically more favorable [1]. Experimentally, this usually manifests itself in even-even nuclei in a sudden drop of the $E(2_1^+)$ energy and the gradual lowering of an excited 0^+ state [2,3], which constitutes the bandhead of the competing configuration. The region of A $\approx$ 100 exhibits one of the most abrupt shape transitions of this type. Experimentally, it was established that the isotopic chains of Sr, Zr, and Mo exhibit a very sudden onset of deformation going from $N = 58$ to $N = 60$ [4–9]. Mass measurements of krypton $Z = 36$ and rubidium $Z = 37$ isotopes were performed [10], labeling $Z = 37$ as the boundary of this region of deformation. Additionally, recent γ spectroscopy identified ^{97}Rb as the lower cornerstone of this phenomenon [11]. In agreement with this, earlier experimental results had established a rather gradual development of collectivity in krypton isotopes with a slow decrease in $E(2_1^+)$ up to $N = 60$ [12,13] and no evidence for low-lying intruder states. However, more recent studies revealed a slightly different behavior for $N \geqslant 60$ [14,15]. In ^{96}Kr, an unexpectedly low value of the ratio $E(4_1^+)/E(2_1^+)$ was determined experimentally [14]. In ^{98,100}Kr, a significant drop of $E(2_1^+)$ was observed, and for ^{98}Kr a low-lying $(0_2^+, 2_2^+)$ state was identified [15]. The discovery of a low-lying $(0_2^+, 2_2^+)$ state in ^{98}Kr, as evidence for a coexisting deformed configuration, also encourages the search for excited bands in the Kr isotopes with $N < 60$ to further investigate the presence of deformed coexisting configurations in this region. To examine this development of shape coexistence in Kr isotopes, different theoretical approaches have been used [13,16]. Most recently, Gogny-D1M calculations were performed by Nomura *et al.* [17] for the even krypton isotopes. For $^{88-92}$Kr, this reveals a defined γ softness that develops into a γ-soft oblate minimum for ^{94}Kr. For the isotopes with $N > 58$, the energy surfaces show a pronounced prolate-oblate shape coexistence further cementing the experimental results. Hence, the changes between ^{94}Kr and ^{96}Kr are crucial for the understanding of the shape evolution in the krypton isotopes specifically and in this region generally.

In this paper, we report on the observation of a new 32(3)-ns isomer at 3444 keV in ^{94}Kr together with several new yrast and nonyrast γ transitions extending the previously known level scheme. Prior to this work, the only published γ transitions in ^{94}Kr were 665.5, 853.2, and 1001.3 keV, measured via Coulomb excitation at the REX-ISOLDE facility by Albers *et al.* [12] and following spontaneous fission of ^{248}Cm with the EUROGAM 2 array by Rząca-Urban *et al.* [18]. On the basis of angular correlation analysis, a spin and parity of 2^+ and of 4^+ were assigned to the levels at 665.5 and 1518.7 keV, respectively, with the remaining transition of 1001.3 keV populating the 4^+ level [18].

II. EXPERIMENT

The measurement, presented in this paper, was performed in 2018 as part of the ν-Ball campaign at the ALTO facility at the IPN Orsay in France, using the ^{238}U(n, f) fast-neutron-induced fission reaction [19,20]. Here, ^{94}Kr was populated much more strongly with a yield of 0.8% as opposed to 0.04% for fission of ^{248}Cm [21]. The directional fast-neutron beam was produced with the neutron source LICORNE [22], which uses the $p(^7\text{Li}, ^7\text{Be})n$ reaction in inverse kinematics. The ^{7}Li beam was provided by the 15-MV Tandem Van de Graaff accelerator in a pulsed mode with a 2-ns pulse width and a repetition period of 400 ns. The ^{7}Li beam entered the hydrogen gas cell of LICORNE through a 2.8-μm tantalum foil. During the experiment a 16-MeV ^{7}Li beam was used together with a 3.5-cm H_2 gas cell with a pressure of 1.2 atm to maximize the neutron flux. The neutrons then impinged on an 81-g ^{238}U sample with a composition of 99.8% ^{238}U and 0.2% ^{235}U produced by JRC-Karlsruhe. The fissile material was arranged in five thin disks over a distance of 8 cm to allow low-energy γ rays to escape from the target. No Doppler correction was required as the fission fragments were stopped in the material. Therefore, the energy resolution of the detectors only depended on their intrinsic resolution giving the spectrometer an excellent resolving power. The ^{238}U sample was placed at a distance of 4 cm to LICORNE to maximize the fission rate. ^{238}U has a fission threshold of $\approx$1.2 MeV and in comparison to ^{235}U a very small fission cross section of 0.5 b at this energy [23]. During the experiment an average primary ^{7}Li beam flux of 2×10^{10}/s was achieved, which translated into a secondary neutron beam of 2×10^6/s and a rate of 10^4 fission events/s. Additionally, a neutron detector was placed behind the setup to measure the neutron energy ($\approx$1.7 MeV) via time-of-flight, but was not relevant to this analysis.

The ^{238}U sample was situated at the center of the ν-Ball array, a novel hybrid high-purity germanium (HPGe)-$LaBr_3$ γ spectrometer that was designed to combine the excellent energy and timing resolution of the two detector types, respectively [20]. A schematic view of the LICORNE chamber and the detector setup can be seen in Fig. 1. During the fission campaign, the array consisted of 24 HPGe Clover detectors, 10 coaxial phase I HPGe detectors, all with bismuth germanium oxide Compton shielding, and 20 $LaBr_3$ detectors without Compton shielding. The phase I detectors were placed in a ring at a backward angle of 133.5°, and the Clover detectors were placed in two rings around 90°. The $LaBr_3$ detectors were mounted in two rings around 40°. Because of the presence of the directional neutron beam, no γ detector was placed at extreme forward angles (<20°) in order to avoid neutron-induced damages to the detectors. Calibration measurements were performed using ^{152}Eu and ^{60}Co standard γ sources. The combined resolution of all HPGe channels was 2.35 keV at 1 MeV, with resolutions of single detectors ranging from 1.7 keV for Clover detectors to 2.9 keV for

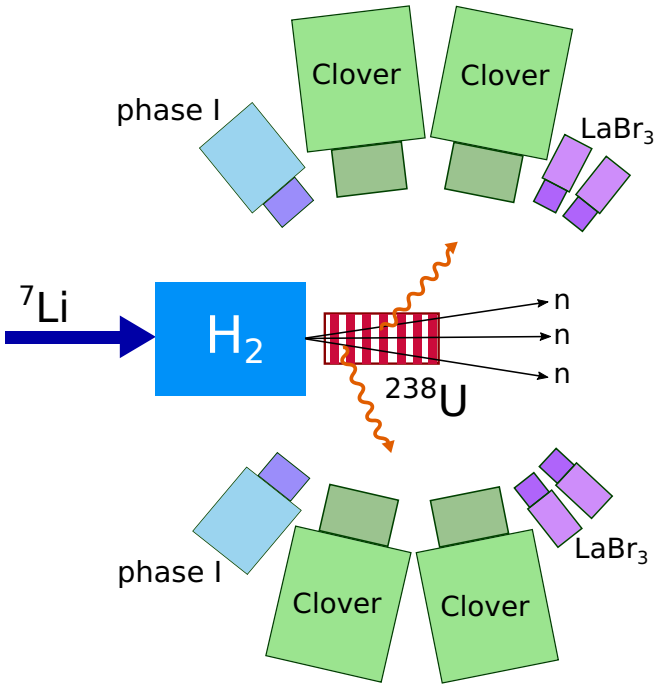

FIG. 1. Schematic drawing of the ν-Ball array, coupled to the LICORNE fast-neutron source. The $p(^7\mathrm{Li}, ^7\mathrm{Be})n$ reaction produced a focused fast-neutron beam that induced fission in the ^{238}U material. The γ rays stemming from the excited fission products were measured with the ν-Ball array, consisting of 10 phase I HPGe, 24 Clover HPGe, and 20 $LaBr_3$ detectors. The solid angle coverage was approximately 70%.

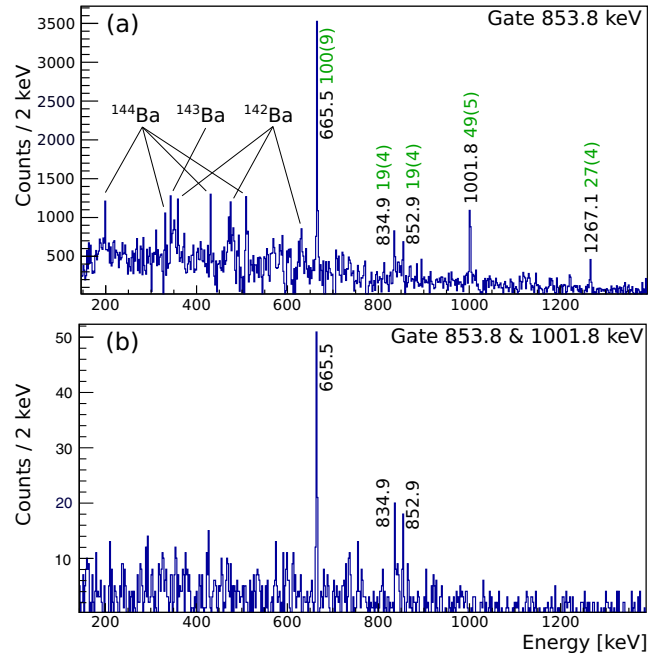

FIG. 2. (a) Background-subtracted energy spectrum coincident to the gate on the 853.8-keV 4_1^+ to 2_1^+ transition in the prompt time window. The efficiency-corrected intensities normalized to the strongest transition at 665.5 keV (green) are shown next to the peaks. Only events where at least three different HPGe detector hits were recorded are considered. (b) The energy spectrum after a second gate on 1001.8 keV is applied.

phase I detectors. A photopeak efficiency of 6.7% at 1.3 MeV for the HPGe detectors was simulated with GEANT4 before the campaign [20]. The measured values were in excellent agreement for energies above 344 keV. For lower energies the efficiency was slightly lower than expected due to absorption in the aluminum gas cell of LICORNE [20]. The measurement was performed in a triggerless mode and the FASTER data acquisition system was used for processing [24]. In total, approximately 216 h of data were taken. In the following, only results from the analysis of the HPGe detectors are presented.

III. DATA ANALYSIS AND RESULTS

The 400-ns pulsed beam makes it possible to investigate prompt and delayed γ transitions separately and in coincidence. For the HPGe detectors, the prompt peak in the timing distribution has a full width at half maximum of $\approx$23 ns, which includes the intrinsic time resolution of the detectors, the beam pulse width, and the time-of-flight differences of the neutrons over the target length. For γ rays emitted outside of the prompt time region, the energy spectra can be cleaned significantly by setting a timing condition of $T \geqslant 35$ ns after the beam pulse, with the higher limit set dependent on the half-life range being investigated. A timing gate of $T \leqslant 35$ ns after beam pulse was used to specifically look for prompt γ rays. Additionally, the background could be reduced significantly by optimizing multiplicity conditions for the number of detected γ rays in the full and in the delayed time windows. In this case, events were built with the total γ multiplicity of $\geqslant$5 and $\leqslant$17 with a minimum of two HPGe detectors fired to select fission and to suppress low-multiplicity events such as inelastic scattering. An additional constraint on the delayed multiplicity was used after the number of delayed transitions was determined.

The prompt background-subtracted energy spectrum produced by a gate on the 4_1^+ to 2_1^+ 853.8-keV transition is presented in Fig. 2(a). The previously published transitions, 665.5 and 1001.3 keV, are the strongest peaks in the spectrum along with several lines from the fission partner isotopes $^{142-144}$Ba. Three additional lines at 834.9, 852.9, and 1267.1 keV are present. With an additional gate on the 1001.8-keV transition [Fig. 2(b)], the peak at 1267.1 keV disappears, which suggests a parallel branch. This will be explored further in the analysis of the delayed time window. The other two peaks remain visible, as can be seen in Fig. 2(b), which proves them to be in coincidence with the 1001.8-keV and 4_1^+ to 2_1^+ transitions. The peak at 852.9 keV is very close in energy to that of the 4_1^+ to 2_1^+ transition of 853.8 keV. However, because this transition is visible when gating on the 4_1^+ to 2_1^+ transition, in any double-gate combination of yrast states, it is assumed that such a transition at 852.9 keV exists. Due to their coincidence relation to the previously established yrast states, we place the 834.9- and 852.9-keV transitions above the three previously known transitions (see Fig. 5). The ordering and tentative spin assignment as (8^+) and (10^+) is clarified by the

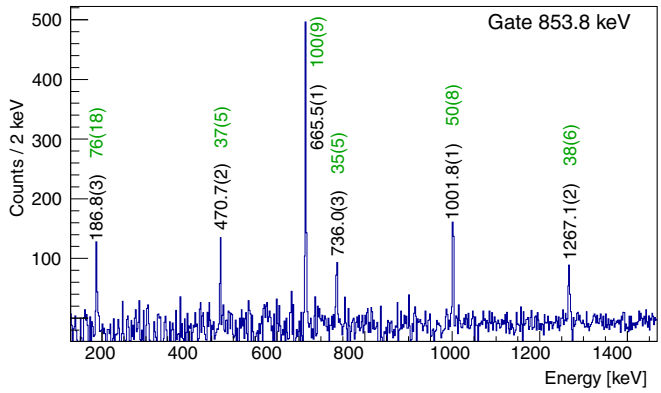

FIG. 3. Background-subtracted energy spectrum coincident with the gate on the 4_1^+ to 2_1^+ 853.8-keV transition in the delayed 35–180 ns time window. The efficiency-corrected intensities normalized to the strongest transition at 665.5 keV (green/gray) are shown next to the peaks.

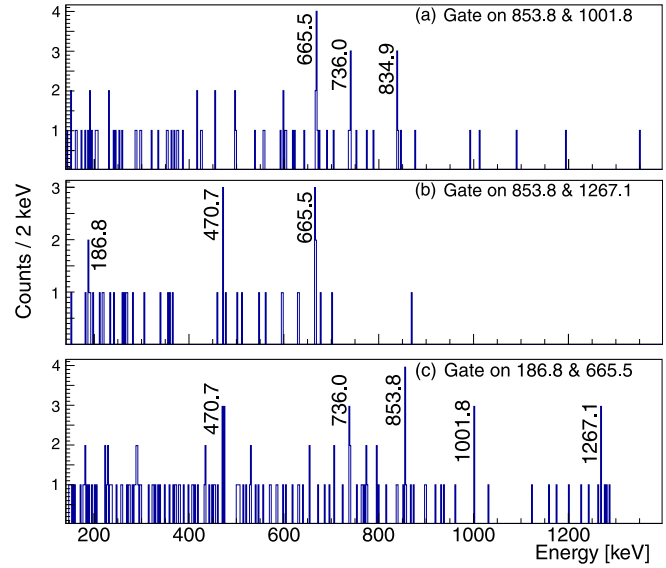

FIG. 4. Double-gated energy spectra in the delayed 35–180 ns time window. (a) Gated on the 853.8- and 1001.8-keV transitions. (b) Gated on the 853.8- and 1267.1-keV transitions. (c) Gated on the 186.8- and 665.5-keV transitions.

analysis of delayed γ transitions in the subsequent discussion. Additionally, three transitions, 665.5, 551.2, and 695.3 keV, were observed in coincidence with each other. Even though 665.5 keV matches the known 2_1^+ to 0_1^+ transition energy, for fission data a second gate on a known transition would normally be necessary to reliably assign these transitions to ^{94}Kr. However, in ^{94}Kr a transition of approximately 550 keV was observed in coincidence with the 665.5-keV transition [25] in the data taken during the 2015 SEASTAR campaign at RIKEN [26]. Therefore, the transitions 551.2 and 695.3 keV are placed in the level scheme as seen in Fig. 5. They are not seen in coincidence with any other prompt or delayed transition.

For the analysis of the delayed γ rays, besides the total multiplicity of $\geqslant 5$ and $\leqslant 17$, the additional constraint on the delayed multiplicity was set with respect to the expected number of delayed transitions in the different isotopes. In Fig. 3, the background-subtracted energy spectrum gated on the 4_1^+ to 2_1^+ transition in a time window of 35–180 ns after a beam pulse with a delayed multiplicity of $\geqslant 2$ and $\leqslant 6$ can be seen. The delayed time window was optimized after the half-life of the new isomer had been determined. Next to three coincident peaks at 665.6, 1001.8, and 1267.1 keV previously visible in the gated prompt spectrum, three additional peaks at 186.8, 470.7, and 736.0 keV show up.

By looking at different delayed double gates, one can observe two parallel decay paths on top of the 4_1^+ to 2_1^+ transition. When comparing the spectra generated by gating on the 4_1^+ to 2_1^+ transition and the 1001.8-keV transition and the 4_1^+ to 2_1^+ transition and 1267.1-keV transition, as seen in Figs. 4(a) and 4(b) respectively, only the 2_1^+ to 0_1^+ 665.5-keV transition remains as coincident to both double gates. If we look at the efficiency-corrected intensities, we find that $I_{853.8} \approx I_{1001.8} + I_{1267.1}$ and $I_{186.8} \approx I_{470.7} + I_{736}$. When double gating on the 186.8-keV and 2_1^+ to 0_1^+ transitions, with the exception of 834.9 keV all other delayed transitions appear in coincidence [see Fig. 4(c)]. With this information, the level scheme was expanded as shown in Fig. 5. Concerning the 834.9-keV line, visible both in the prompt energy spectra and the double-gated delayed spectrum in Fig. 4(a), we assume that a nonobserved 88-keV transition connects the isomeric 3444-keV level with the (8^+) level at 3356 keV. With our setup, a transition of this energy is very unlikely to be observed due to the low efficiency at that energy. The high Z and the thickness of the target material attenuate low-energy γ rays strongly.

To determine the half-life of the 3444-keV isomer, the data were sorted into a $\gamma\gamma T$-cube to obtain the timing distribu-

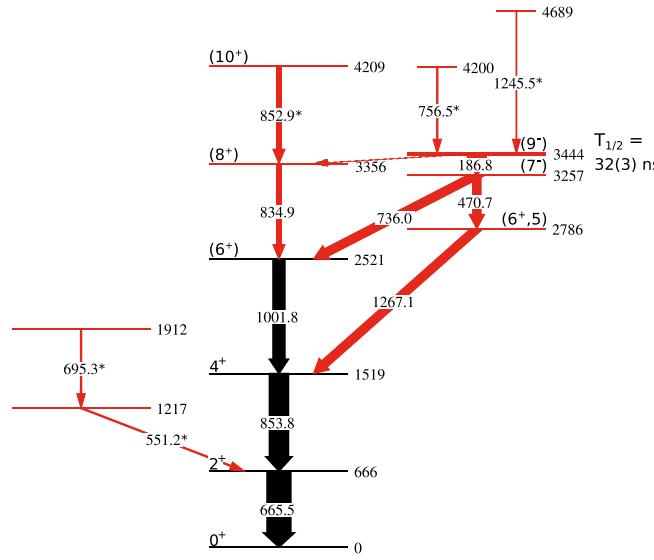

FIG. 5. Level scheme constructed for ^{94}Kr. Energies are given in keV. The widths of the transitions arrows correspond to their efficiency-corrected intensities. New transitions and levels are shown in red (gray). Transitions denoted by an asterisk are only observed in the prompt time window.

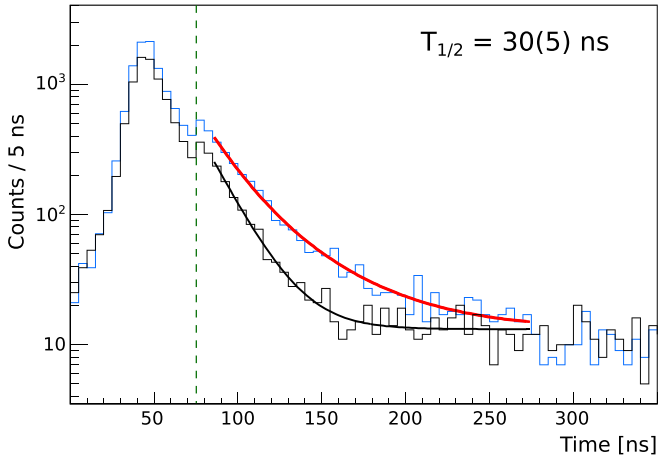

FIG. 6. Time spectrum and fitted decay curve used to determine the half-life of the 3444-keV isomer. For this spectrum, only events that have a delayed multiplicity of $\geqslant 2$ and $\leqslant 6$ in the delayed time region (beyond the dashed line) were considered. The decay curve is fitted with an exponential decay function (thick red/gray curve) together with a time-dependent background (black curve). To maximize statistics the time distributions of different γ-ray coincidences below the isomer were added up to one decay curve (thin blue/gray curve).

tion of the intensities of the delayed coincidences of ^{94}Kr. As test cases, the isotopes ^{134}Te and ^{95}Sr with well-known isomers with half-lives of 164.1(9) and 21.9(5) ns [27,28], respectively, were used for every step to verify the analysis method. For these cases, we obtained half-lives of 166(6) and 21.0(5) ns, in excellent agreement with the literature values.

Fig. 6, the time distribution used for the determination of the isomer half-life is shown. The timing spectra for the 665.5/853.8, 665.5/1001.8, 665.5/470.7, 853.8/470.7, and 853.8/1001.8 keV prompt coincidences of transitions, which are situated below the 3444-keV isomer, were added up to maximize statistics. The other combinations of transitions below the isomer were not used here due to low statistics. The second, smaller peak in the time distribution at 75 ns is a result of the artificial boundary introduced by defining and limiting the delayed multiplicity. The half-life was obtained by simultaneously fitting the time-dependent summed background spectrum of the coincidences (see black histogram in Fig. 6) together with the nonsubtracted time spectrum of the five coincidence pairs [see thin blue (gray) histogram in Fig. 6] using the maximum likelihood method in the same manner as in Ref. [29]. By varying the energy ranges of the background, the systematic uncertainty could be estimated. Together, this yields a half-life of 30(5) ns.

Figure 7 shows the background-subtracted energy spectrum in the prompt time window produced by double gating on the delayed transition pairs 665.5/853.8, 665.5/1001.8, 665.5/1267.1, 665.5/470.7, 853.8/470.7, 853.8/1001.8, and 853.8/1267.1 keV below the 3444-keV isomer in the delayed time window 35–180 ns and adding up the coincident prompt spectra. The strongest peaks in the resulting spectrum are the lowest transitions in the partner fission isotopes $^{142-144}$Ba (as also seen in Fig. 2), 511 keV, and two new transitions at 756.6

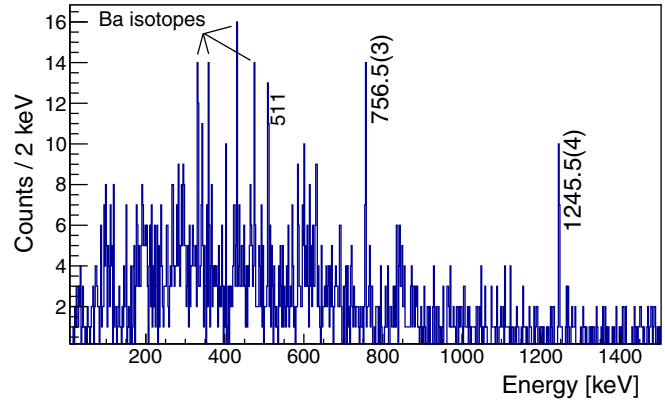

FIG. 7. Background-subtracted prompt energy spectrum generated by double gating on coincidences of delayed γ transitions below the 3444-keV isomer in the 35–180 ns time window.

and 1245.5 keV. Accordingly, these two transitions can be placed on top of the isomer in the level scheme. Because they are not seen in coincidence to each other, we place them in parallel to each other, as seen in Fig. 5. Because these new transitions are feeding the isomeric state, the time difference between them and the delayed transitions depopulating the isomer can be used for a second determination of the isomeric half-life. In Fig. 8, the prompt-delayed $\gamma\gamma\Delta T$-spectrum for the isomer is shown. To maximize statistics, the time differences between both prompt transitions, 756.6 and 1245.5 keV, feeding the isomer, and the transitions 665.5, 853.8, 1001.8, and 1267.1 keV, below the isomer, were added up. As above, the half-life was obtained by simultaneous fitting of the time-dependent summed background spectrum and the nonsubtracted ΔT spectrum of the prompt-delayed pairs. This yields a half-life of 33(4) ns in accordance with the half-life obtained from Fig. 6. Due to the independence of the two results, we can take the weighted average, which results in $T_{1/2} = 32(3)$ ns. The measurement of this short-lived iso-

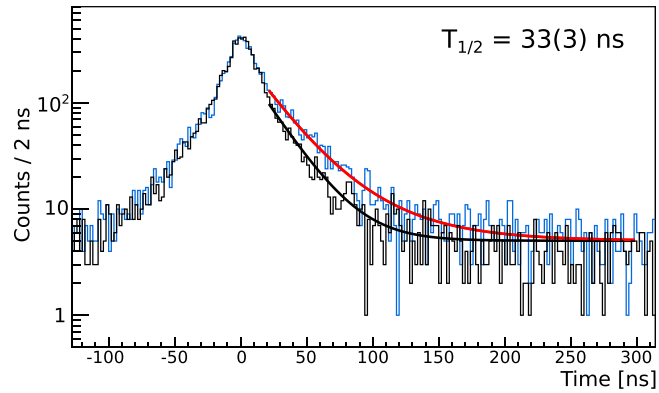

FIG. 8. Prompt-delayed ΔT spectrum of prompt transitions populating and delayed transitions depopulating the 3444-keV isomer. The decay curve is fitted with an exponential decay function (thick red curve) together with a time-dependent background (thick black curve). To gain statistics, several prompt-delayed transition combinations were added up to one decay curve (thin blue/gray).

mer demonstrates the capabilities of the ν-Ball array in this half-life range, complementary to in-flight facilities where this time range is not always accessible.

IV. DISCUSSION

The new level scheme of ^{94}Kr is shown in Fig. 5. The excitation energies are indicated next to each level. The widths of the arrows are proportional to the efficiency-corrected intensities obtained for the transitions. The two new transitions 834.9 and 852.9 keV, observed in the prompt time window (see Fig. 2) to be coincident with the previously published yrast transitions [18], were assigned to be feeding the (6_1^+) and (8_1^+) states. The ordering was deduced from the prompt coincidence analysis (see Fig. 2) and the delayed coincidence analysis (see Fig 4). The 834.9-keV transition is also observed in the delayed time window and therefore has to be below the isomeric state at 3444 keV. The state at 4209 keV, depopulated by the 852.9-keV transition in the prompt time window, needs to have a spin of $J_{4209} > 8$, with the most likely candidate being (10_1^+). The level at 2786 keV decays to the 4_1^+ level at 1519 keV, while a transition to the 6_1^+ level at 2521 keV was not observed. Thus, the most probable spin-parity assignments, producing the lowest possible multipole radiation, for the 2786-keV state are $(5,6^+)$. The higher level at 3257 keV, right below the isomeric state, decays to the 6_1^+ level at 2521 keV and to the $(5,6^+)$ level at 2786 keV, not to the 4_1^+ or 2_1^+ level, which suggests a spin of $J_{3257} > 6$. On top of the level, there is the 186.8 keV transition which also depopulates the isomer. Calculating the reduced transition strength based on a single-branch with the TRANSNUCULAR code [30], a transition multipolarity of $\geqslant 3$ can be excluded. For a single branch $E2$ transition with this energy, this yields 2.8(3) W.u. while for $E1$, $M1$, and $M2$ transitions the results are either much too low or much too high to be reasonably compatible with physical expectations. The most likely $E2$ character of this transition suggests $9^{+/-}$ and $7^{+/-}$ states as the most probable assignments for the 3444-keV isomer and the 3257-keV state, respectively. In fact, in the neighboring isotone ^{96}Sr, there is a well-known 40-ns isomeric 9^- state depopulated via $E2$ and $E1$ transitions [32,33]. This has been well described by shell-model calculations suggesting a dominant neutron $(g_{7/2}, h_{11/2})_{9^-}$ configuration [33]. This resembles the situation observed in our ^{94}Kr level scheme supporting the tentative spin assignments of (9^-), (7^-), and (8^+) for the corresponding states. Additionally in ^{96}Sr, there is a prompt cascade, $10^+ \rightarrow 8^+ \rightarrow 6^+$, bypassing the isomer [32,34] in further support of our tentative spin assignment for the 4209-keV state to be a (10^+). Furthermore, very recently in the lower $N = 58$ isotone ^{92}Se, a long-lived 15.7-μs isomeric state at 3072 keV was measured with the HPGe-spectrometer EURICA [35]. The isomer has been observed to decay only via a 67-keV $E2$ transition with a transition strength of around 1 W.u. The authors also assigned this as a tentative (9^-) state decaying into to a (7^-) state, assuming single-particle character and identifying the two states as oblate two-quasiparticle neutron configurations $7^- = 11/2^-[505] \otimes 3/2^+[402]$ and $9^- = 11/2^-[505] \otimes 7/2^+[404]$ [35]. The Nilsson orbitals were determined with Gogny cranked Hartree-Fock-Bogoliubov (CHFB) calculations [31].

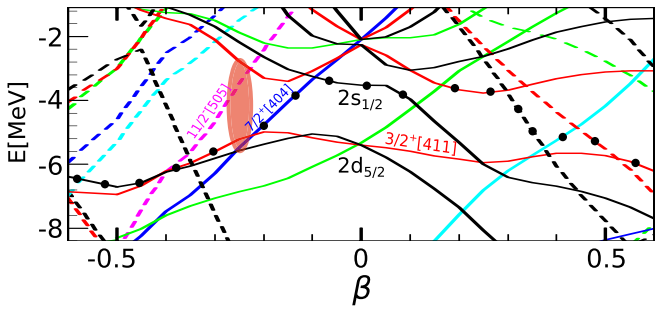

FIG. 9. Partial Nilsson diagram for neutrons. The Fermi surface for $N = 58$ is denoted with black dots. Adapted from Delaroche *et al.* [31], obtained with Gogny CHFB calculations.

In Fig. 9, we can see the corresponding Nilsson diagram for neutrons near the Fermi level of ^{94}Kr, which is very similar to the one for ^{92}Se. At an oblate deformation of $\beta \approx -0.22$, the same two-quasiparticle states exist as in ^{92}Se (see red area in Fig. 9). Thus, the decay from (9^-) to (7^-) in ^{94}Kr can be interpreted as a transition of a neutron from the $7/2^+[404]$ to the $3/2^+[402]$ level. The orbitals involved are labeled in Fig. 9. From the microscopic point of view, the Nilsson 9^- two-quasiparticle configuration corresponds to the shell-model $(g_{7/2}, h_{11/2})_{9^-}$ one. However, while interacting shell-model calculations are in the spherical basis and deformation parameters can only be calculated in a framework of shape invariants, the Nilsson model allows for an estimation of the deformation parameter β based on the observation of unique single-particle configurations. In ^{94}Kr, the oblate deformation of the isomeric state, as deduced from the assumed Nilsson configurations in Fig. 9, is nearly the same as the one of the ground state ($\beta \approx -0.26$) as predicted by the same calculations [31]. To estimate the reduced transition strengths for the isomeric decay branches, we assume pure $E1$ and $E2$ decay branches similar to ^{96}Sr. The branching ratio of $I_{88} \approx \frac{1}{2} I_{186.8}$ is derived by analyzing the intensities of the 470.7-, 736.0-, and 834.9-keV transitions in Fig. 4. Due to the low statistics, intensity uncertainties of 50% were assumed and propagated in the calculation. Thus, when considering a two-branch decay of the isomer with an 88-keV $E1$ transition and a 186.8-keV $E2$ transition, reduced transition strengths of $B(E1) = 4^{+3}_{-2} \times 10^{-6}$ W.u. and $B(E2) = 1.8^{+0.5}_{-0.5}$ W.u. are obtained.

To discuss aspects of the nuclear structure in the $N = 58$ isotones under the assumption that the tentative spin and parity assignments are correct, partial level schemes of ^{92}Se, ^{94}Kr, and ^{96}Sr are shown in Fig. 10. While in ^{94}Kr and ^{96}Sr the excitation energies and relative position of the 9^- and 7^- levels are relatively constant, both the excitation energies and their separation slightly decrease in ^{92}Se. In all three isotopes, the reduced $E2$ transition strengths of about 1 W.u. show a single-particle character for the isomeric decay. In ^{94}Kr and ^{96}Sr, a competing $E1$ branch is observed. This is not the case in ^{92}Se, most probably due to the higher relative position of the 8^+ state as suggested by the up-sloping trend of the corresponding states in ^{96}Sr and ^{94}Kr (see Fig. 10).

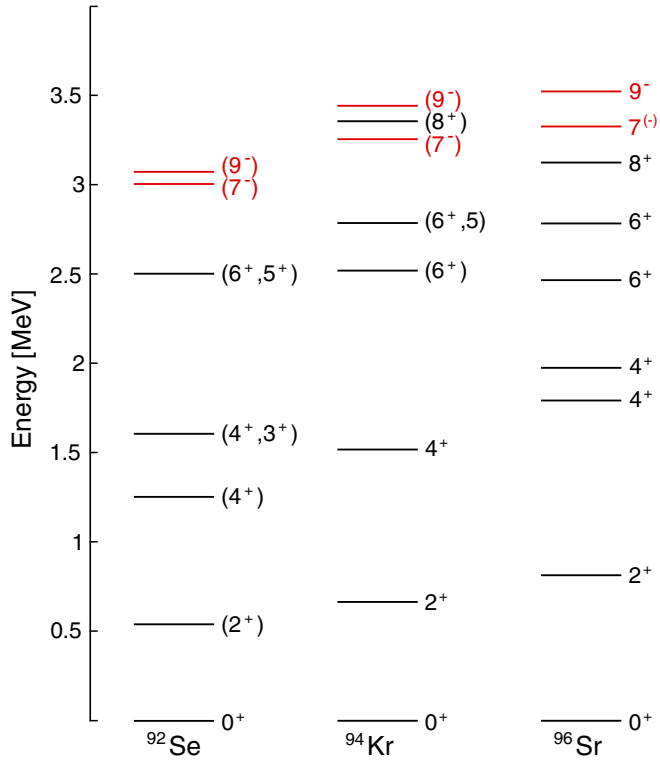

FIG. 10. Comparison of partial level schemes of ^{92}Se, ^{94}Kr, and ^{96}Sr. Data are from this work and Refs. [18,33,35,36].

In Wu *et al.* [34], relative $B(E2)$ values for the internal decay of some states in ^{96}Sr were derived based on the corresponding branching ratios and normalized to one of the transitions strengths. The relative $B(E2)$ values from the yrast 6^+ to the two 4^+ states in ^{96}Sr indicated a mixing of the $4^+_{1,2}$ states [34], while in ^{92}Se the calculated relative $B(E2)$ values suggest no mixing of the two 4^+ states based on the branching ratio observed by Lizarazo *et al.* [35]. Similarly, we obtained relative $E1$ transition strengths for the $7^- \rightarrow 6^+_{1,2}$ transitions in ^{94}Kr and ^{96}Sr. In ^{94}Kr, the $B(E1; 7^- \rightarrow 6^+_1)$ is 26(1)% of the $B(E1; 7^- \rightarrow 6^+_2)$, while in ^{96}Sr, it is only 5(1)%. This implies a much greater mixing between the two 6^+ states in ^{94}Kr compared to ^{96}Sr. In ^{92}Se, only one (6^+) state was observed, though from the relatively constant excitation energies of the 6^+ states in ^{94}Kr and ^{96}Sr, one would expect a similar structure.

V. CONCLUSIONS

In conclusion, this work presents the first observation of an isomeric state in ^{94}Kr, measured using the novel hybrid spectrometer ν-Ball with its unique combination of a pulsed beam and fast-neutron-induced fission of ^{238}U. Reduced $E1$ and $E2$ transition strengths for the isomer decay branches were extracted. The isomer is interpreted as being built on a two-quasiparticle neutron state consistent with Gogny CHFB calculations, presenting an isomeric spin structure very similar to that in the neighboring isotones ^{92}Se and ^{96}Sr. Additionally, the level scheme was expanded significantly, allowing us to discuss nuclear structure by looking into the level systematics of $N = 58$ isotones and mixing of states by comparing relative transition strengths.

ACKNOWLEDGMENTS

We thank the accelerator staff of the ALTO facility at the IPN Orsay for providing a stable beam and continuous support. This work is supported by the Deutsche Forschungsgemeinschaft (DFG) under Grant No. BL 1513/1-1 and by the BMBF under Grants No. 05P15RDFN1 and No. 05P19RDFN1. This work was partially funded by the Spanish government via Projects FPA2015-65035-P and RTI2018-09886 8-B-I00. This work was partially supported by the STFC UK Nuclear Data Network, the STFC (Grants No. ST/L005743/1 and No. ST/P005314), the University of Surrey Marion Redfearn Trust. A.B., M.B., P.I., S.J., and P.H.R. acknowledge support from the UK Department of Business, Energy and Industrial Strategy (BEIS) via the National Measurement System. This work was supported by EC funding for External Research Teams within the HORIZON2020 Program of the European Commission TransNational Access to ALTO under the Integrated Infrastructure Initiative European Nuclear Science and Applications Research 2 (ENSAR2) Grant Agreement No. 654002. The use of germanium detectors from the GAMMAPOOL is acknowledged.

[1] K. Heyde and J. L. Wood, Rev. Mod. Phys. **83**, 1467 (2011).
[2] F. Schussler, J. A. Pinston, E. Monnand, A. Moussa, G. Jung, E. Koglin, B. Pfeiffer, R. V. F. Janssens, and J. van Klinken, Nucl. Phys. A **339**, 415 (1980).
[3] T. A. Khan, W. D. Lauppe, K. Sistemich, H. Lawin, G. Sadler, and H. A. Selic, Z. Phys. A **283**, 105 (1977).
[4] E. Cheifetz, R. C. Jared, S. G. Thompson, and J. B. Wilhelmy, Phys. Rev. Lett. **25**, 38 (1970).
[5] F. K. Wohn, J. C. Hill, R. F. Petry, H. Dejbakhsh, Z. Berant, and R. L. Gill, Phys. Rev. Lett. **51**, 873 (1983).
[6] W. Urban *et al.*, Eur. Phys. J. A **22**, 241 (2004).
[7] C. Kremer *et al.*, Phys. Rev. Lett. **117**, 172503 (2016).
[8] E. Clément *et al.*, Phys. Rev. Lett. **116**, 022701 (2016).
[9] T. Togashi, Y. Tsunoda, T. Otsuka, and N. Shimizu, Phys. Rev. Lett. **117**, 172502 (2016).
[10] S. Naimi *et al.*, Phys. Rev. Lett. **105**, 032502 (2010).
[11] C. Sotty *et al.*, Phys. Rev. Lett. **115**, 172501 (2015).
[12] M. Albers *et al.*, Phys. Rev. Lett. **108**, 062701 (2012).
[13] M. Albers *et al.*, Nucl. Phys. A **899**, 1 (2013).
[14] J. Dudouet *et al.*, Phys. Rev. Lett. **118**, 162501 (2017).
[15] F. Flavigny *et al.*, Phys. Rev. Lett. **118**, 242501 (2017).
[16] T. R. Rodríguez, Phys. Rev. C **90**, 034306 (2014).
[17] K. Nomura, R. Rodríguez-Guzmán, Y. M. Humadi, L. M. Robledo, and H. Abusara, Phys. Rev. C **96**, 034310 (2017).
[18] T. Rząca-Urban *et al.*, Eur. Phys. J. A **9**, 165 (2000).
[19] N. Jovančević *et al.*, Acta Phys. Pol., B **50**, 297 (2019).

[20] M. Lebois, N. Jovančević, D. Thisse, R. Canavan, D. Étasse, M. Rudigier, and J. N. Wilson, Nucl. Instrum. Methods Phys. Res., Sect. A **960**, 163580 (2020).
[21] T. R. England and B. F. Rider, Technical Reports No. LA-SUB-94-170, No. ON: DE95003450, No. TRN: 95:000123, Los Alamos National Lab., NM United States, doi: 10.2172/10103145.
[22] M. Lebois, J. N. Wilson, P. Halipré, B. Leniau, I. Matea, A. Oberstedt, S. Oberstedt, and D. Verney, Nucl. Instrum. Methods Phys. Res., Sect. A **735**, 145 (2014).
[23] F. Tovesson, A. Laptev, and T. S. Hill, Nucl. Sci. Eng. **178**, 57 (2014).
[24] D. Etasse *et al.* http://faster.in2p3.fr.
[25] K. Moschner (private communication); R.-B. Gerst *et al.* (unpublished).
[26] P. Doornenbal *et al.*, RIKEN Accel. Prog. Rep. **49**, 35 (2016).
[27] A. Sonzogni, Nucl. Data Sheets **103**, 1 (2004).
[28] S. Basu, G. Mukherjee, and A. Sonzogni, Nucl. Data Sheets **111**, 2555 (2010).
[29] G. Häfner *et al.*, Phys. Rev. C **100**, 024302 (2019).
[30] N. Saed-Samii, Computer code TRANSNUCULAR (private communication).
[31] J.-P. Delaroche, M. Girod, J. Libert, H. Goutte, S. Hilaire, S. Péru, N. Pillet, and G. F. Bertsch, Phys. Rev. C **81**, 014303 (2010).
[32] W. Urban *et al.*, Nucl. Phys. A **689**, 605 (2001).
[33] T. Rząca-Urban, K. Sieja, W. Urban, F. Nowacki, J. L. Durell, A. G. Smith, and I. Ahmad, Phys. Rev. C **79**, 024319 (2009).
[34] C. Y. Wu, H. Hua, D. Cline, A. B. Hayes, R. Teng, R. M. Clark, P. Fallon, A. Goergen, A. O. Macchiavelli, and K. Vetter, Phys. Rev. C **70**, 064312 (2004).
[35] C. Lizarazo *et al.*, Phys. Rev. Lett. **124**, 222501 (2020).
[36] S. Chen *et al.*, Phys. Rev. C **95**, 041302 (2017).